The Cryosphere Discuss., 6, 1181–1204, 2012
www.the-cryosphere-discuss.net/6/1181/2012/
doi:10.5194/tcd-6-1181-2012

The Cryosphere Discussions

Surge dynamics on Bering Glacier, Alaska, in 2008–2011

E. W. Burgess[1], **R. R. Forster**[1], **C. F. Larsen**[2], **and M. Braun**[3]

[1]Department of Geography, University of Utah, Salt Lake City, Utah, USA
[2]Geophysical Institute, University of Alaska Fairbanks, Fairbanks, Alaska, USA
[3]Department of Geography, Friedrich-Alexander-University Erlangen-Nürnberg, Germany

Received: 21 February 2012 – Accepted: 1 March 2012 – Published: 21 March 2012

Correspondence to: E. W. Burgess (evan.burgess@geog.utah.edu)

Published by Copernicus Publications on behalf of the European Geosciences Union.

Abstract

A 2008–2011 surge of Bering Glacier, Alaska is examined using observations of surface velocity and surface elevation change. Velocity measurements are obtained using synthetic aperture radar (SAR) offset tracking and elevation data are obtained from the University of Alaska Fairbanks LiDAR altimetry program. Bering Glacier began to surge in May 2008 and had two phases of accelerated flow. The first phase accelerated progressively for at least 10 months and reached peak observed velocities of $\sim 7\,\mathrm{m\,d^{-1}}$. Results suggest that during the quiescent phase, prior to the surge, periods of accelerated flow increased driving stresses up to 70 % in a ~ 10 km-long section of the Lower Bering. When the first phase of the surge initiated, synchronous acceleration occurred throughout much of the glacier length, indicating widespread pressurization of the bed, but the largest accelerations initiated at the location where driving stress built up during quiescence. From there, rapid flow velocities propagated upstream and downstream across much of the glacier length and transpired as small, transient and unorganized propagation fronts. The second phase occurred in 2011 and was of comparable scale to the surge in 1993–1995, with velocities exceeding $9\,\mathrm{m\,d^{-1}}$ or ~ 18 times quiescent velocities.

1 Introduction

Glacier surging is a quasi-periodic acceleration of a glacier (called a "surge") to velocities many times "normal" flow (Meier and Post, 1969; Raymond, 1987; Harrison and Post, 2003). Surge events are associated with high basal water pressures that reduce the amount of basal shear stress a glacier bed can support, thus allowing the glacier to slide rapidly on its bed surface. Driving stress (τ_d) is dependent on glacier thickness (h) and very sensitive to glacier surface slope angle (α).

$$\tau_\mathrm{d} = \rho g h \sin\alpha \quad (1)$$

TCD
6, 1181–1204, 2012

At the end of a surge, redistributed mass thickens the terminus and thins upstream, thus reducing the glacier slope angle and reducing the driving stress. Over time, the driving stress can increase again though thickening and steepening. Variegated Glacier, AK, for example, had quiescent flow speeds slower than steady state along most of its length, causing steepening and increased driving stress across most of the glacier until the surge initiated in 1982 (Raymond, 1987; Raymond and Harrison, 1988). During quiescent phase, as a glacier undergoes changes in geometry, flow velocities adjust in response to the changes in stress regimes. In fact, it is not uncommon for surging glaciers to have small acceleration events during quiescent phases (Meier and Post, 1969; Raymond, 1987; Harrison and Post, 2003; Raymond and Harrison, 1988).

The Bering Glacier System (BGS) (Fig. 1) is the largest mountain glacier in the world and the largest surge-type glacier outside of the Greenland and Antarctic ice sheets (Molnia, 2008), accounting for approximately 4 % of the ice area in Alaska (Beedle et al., 2008; Berthier et al., 2010) and approximately 6 % of the ice loss (Arendt et al., 2002). Herein, we refer to the "Bering" as the portion of the BGS from 90 km to the terminus and the "Bagley Ice Valley" (BIV) as the portion from 0–80 km (Fig. 1). The BGS has been steadily retreating over the past 100 yr despite episodic advances during surge events in 1900, 1920, 1938–1940, 1957–1960, 1965–1967 and 1993–1995 (Post, 1972; Molnia, 2008). Both the 1965–1967 and 1993–1995 surge events can be characterized as multi-phased events, beginning with a high velocity event, followed by a period of near stagnant ice, followed by another high velocity event (Harrison and Post, 2003; Molnia, 2008).

The 1993–1995 event is the only BGS surge with quantified flow velocities; these results are worthy of summary to place the current surge in context. Surge onset occurred $\sim$ 135 km from the ice divide (Roush, 2003) (Fig. 1). Maximum flow velocities were $\sim$ 10–20 m d^{-1} (Roush, 2003) near the terminus and up to 5 m d^{-1} in the lower BIV (Fatland and Lingle, 2002). No velocity data were able to confirm the existence of an organized surge front propagating upstream or downstream. A leading surface undulation propagated downstream at $\sim$ 100 m d^{-1} (Roush, 2003). Upstream propagation was

TCD
6, 1181–1204, 2012

less clear. Fatland and Lingle (1998) found a delay between surge onset on the Lower Bering (~ 130 km) and a subsequent acceleration of the West Bagley (WB)(Fig. 1), which lies ~ 60 km upstream. Assuming that the delay was due an upstream propagation front originating from the surge onset location, Fatland and Lingle (1998) estimated the upstream propagation velocity was 200–500 m d^{-1}. Fatland and Lingle (1998) also considered the possibility that the WB accelerated because of a linked sub-glacial hydrologic system and may not have been a classic propagating surge front as observed on the Variegated Glacier (Kamb et al., 1985; Raymond, 1987).

During the 1993–1995 surge, Fatland and Lingle, (2002) found a distinct longitudinal change in ice dynamical behavior at a point just downstream of the Jeffries Glacier confluence, 45 km west of the BGS/Seward ice divide (Fig. 1). East of this point in 1994, acceleration rates were temporally-uniform and longitudinal acceleration differed little from quiescent velocities. West of this point, acceleration rates fluctuated rapidly (on 3-day timescales) and strong longitudinal acceleration occurred where uniform velocities existed prior to the surge. Short-term surface elevation changes, possibly indicative of transient sub-glacial water, were also more abundant downstream of this point during the 1993–1995 surge (Fatland and Lingle, 2002).

2 Data and methods

2.1 SAR offset tracking

We use L and C-Band SAR platforms to generate ice displacement fields via offset/speckle tracking methods (Strozzi et al., 2002; Gray et al., 1998; Michel and Rignot, 1999). We use PALSAR ALOS Fine Beam (46-day repeat), RADARSAT Fine Beam (24-day repeat) ERS Ice Phases (3-day repeat) and TerraSAR-X StripMap (11-day repeat). Acquisitions were screened to obtain pairs with temporal baselines of 1 or 2 orbit intervals and perpendicular baselines < 400 m for RADARSAT and ERS, < 1000 m for PALSAR and < 20 m for TerraSAR-X. We obtained a total of 77 frames, providing 40

TCD
6, 1181–1204, 2012

pairs acquired between 2006 and 2010, 1 TerraSAR-X pair in 2011, and 17 ERS pairs acquired during the 1993–1995 surge (same data as used by Fatland and Lingle, 1998, 2002). Pairs could not be obtained at regular intervals due to poor data availability. Summer pairs were generally not utilized because SAR offset tracking was found to be ineffective during extensive melt, though 2 PALSAR pairs did yield usable displacement fields. The single July TerraSAR-X pair, with an 11-day repeat, also produced good results.

SLC pairs were co-registered using intensity cross-correlation optimization offset tracking within GAMMA® software (Strozzi et al., 2002) or SLC products were used as deliverd by the satellite facility (TerraSAR-X). This method uses statistical correlation to quantify the displacement (offset) of pixel patterns between two images. For each image pair, we derived offsets on stable ground adjacent to glaciers and assumed the offset vector field represents image co-registration. A polynomial function was fit to this offset field and then subtracted from the offsets observed on glaciers in the same image pair. The BGS and surrounding ice is extensive enough to cover most of a single SAR frame (~ 70 km × 80 km); in these cases, glaciated ridgelines were allowed into the image co-registration in order to obtain an accurate offset polynomial. Related errors are discussed in Sect. 3.3.

Ice displacements were generated from the SLCs using the same intensity cross-correlation offset tracking method used for the initial co-registration, but with smaller window sizes. No terrain correction was applied, as resultant uncertainties were small (Sect. 3.3). SLCs were oversampled by a factor of two and all offsets with signal-to-noise ratios (Strozzi et al., 2002) below 6.0 were eliminated. We identified optimum search window sizes by testing throughout the parameter space; optimum sizes were 96 × 156 pixels (nominally, 721 m × 726 m in range and azimuth) and 100 × 200 pixels (nominally, 748 m × 629 m), for RADARSAT and PALSAR, respectively. For TerraSAR-X we used a size of 256 × 256 pixels (232 m × 474 m).

In a few cases, slightly larger windows were used to improve results in areas of poor correlation. Results were not dependent on window size as long as the window was

TCD
6, 1181–1204, 2012

not large enough to extend through shear zones or onto stable ground. Shear zones on Bering Glacier are generally wider than 1.5 km (Fatland and Lingle, 2002).

Erroneous offsets were eliminated, first with an automated filtering routine and then manually. Displacements were geocoded using the ASTER GDEM and SAR imaging geometry. All geocoded displacements were gridded onto the same 30 m UTM grid for comparison. Strain rates were computed following Nye (1959) and Bindschadler et al. (1996). Ice displacements were extracted along centerline longitudinal profiles for the BGS, WB (Figs. 1 and 2) and Jefferies/Tana glaciers (profile not shown). Locations along these profiles will, herein, be referenced using the scales in Fig. 1. For purposes of clarity, we divert the BGS profile off the centerline from 115 to 140 km to circumvent data voids (Fig. 1).

We estimate our velocity uncertainty for each image pair by using the same offset tracking method (Strozzi et al., 2002) on stable-ground where offsets are assumed to be zero and any measured offset represents an error. Suitable areas for uncertainty estimates were manually delineated in each pair. Areas with steep topography, with visible geometric distortion (foreshortening, layover, or shadowing) in the SAR images, were excluded. These uncertainty estimations address errors associated with image co-registration, the lack of terrain correction, and the signal-to-noise ratio accepted in the offset tracking routine.

2.2 Airborne altimetry

The University of Alaska Fairbanks (UAF) Laser Altimetry Program has flown centerline repeat surface elevation profiles on over 200 glaciers across Alaska and adjoining Canada since 1993 (Echelmeyer et al., 1996; Arendt et al., 2002, 2006). Centerline profiles of the BGS were flown in June 1995 and 2000, in August 2000, 2003, 2007, in September 2008 and in August 2009, and 2010. These surveys used two different techniques: a nadir pointing laser (1995–June 2009) and, more recently, a swath mapping LiDAR as part of NASA's Operation IceBridge (August 2009–2010) (Koenig et al., 2010).

TCD
6, 1181–1204, 2012

The nadir pointing laser system results in a single track of surveyed points along the flight path, spaced roughly 1.0 to 1.5 m apart, whereas the LiDAR system results in a 500 m wide swath with roughly one surveyed point per square meter. Vertical accuracy of the surveyed points ranges from ±0.1 to ±0.3 m, dependent largely upon the quality of the trajectory solution for the aircraft (position and orientation from GPS and inertial measurement unit onboard the aircraft). To calculate changes in elevation between nadir pointing laser surveys, we followed techniques and error estimations as described by Arendt et al. (2008). Calculating elevation changes between nadir laser surveys and LiDAR surveys, and between LiDAR to LiDAR surveys is done by interpolating the later survey onto a 5 m gridded surface, then sampling that surface at the earlier survey's points. In both of these cases, the inherent ambiguity between local slope (from the old point to the new point) and elevation changes is greatly mitigated relative to comparing two single tracks of points. To minimize seasonal effects on elevation changes, each interval was flown within 8 days of the date of the previous survey, with the exception of 39 days (late) in 2008.

3 Results

3.1 Efficacy of PALSAR in maritime climates

Not all SAR pairs produced useable offset results; the climate in Southeast Alaska rarely leaves a glacier surface unaffected by heavy snowfall or significant melt over a ∼ 1 month interval. We find that, in this environment, temporal de-correlation is event (storm) based, rather than a gradual process, thus avoiding orbit intervals that span extreme storms or melt events can increase chances of obtaining good velocity results. In this climate, C-Band and X-Band sensors generally require surface definition such as crevassing and can't track speckle alone (ERS ice-phases with shorter repeats excluded), which limits spatial coverage significantly. In contrast, L-Band was extremely robust and able to track speckle reliably in this climate despite PALSAR's longer 46-day

TCD
6, 1181–1204, 2012

orbit interval. This strength is due to the longer wavelength providing deeper penetration and more stable scattering from subsurface snow and firn. TerraSAR-X was also effective because of the extremely short orbit interval (11-days) and high spatial resolution. However, it may be limited in observing slower moving ice. X-Band decorrelates relatively quickly, thus requiring shorter intervals, which reduces accuracy.

3.2 Offset tracking uncertainties

We calculated uncertainty offset fields for 28 PALSAR pairs and 13 RADARSAT pairs. An average of 5030 offset values were calculated per image pair. The stable-ground offsets/errors are not normally distributed, primarily because of extreme outliers. Thus, we use robust statistics including the median, interquartile range (IQR) and normalized median absolute deviation (MADn, a robust equivalent to standard deviation) (Maronna, 2006) to describe stable-ground offset fields (Table 1). Dispersion metrics quantify stochastic uncertainty, while the mean absolute median provides an estimate of bias.

Both platforms have mean absolute median values $< 0.01\,\mathrm{m\,d^{-1}}$ in both range and azimuth directions; random errors are larger (Table 1). PALSAR has larger stochastic errors in the range direction than in azimuth, whereas RADARSAT has isotropic stochastic error. PALSAR also has significantly larger perpendicular baselines than RADARSAT, thus it is likely that the larger errors in the range direction are a consequence of our lack of topographic corrections. This source of uncertainty is still too small to affect results.

During the surge, there is extreme velocity variability that has the appearance of noise in longitudinal profiles (visible in Fig. 2). Visual inspection of the velocity maps used to generate the profiles, suggests that much of the spatial variability is indeed real and not noisy results. However, rapid changes in surface conditions during the surge leads to a few errant velocity vectors that appear as noise in the profiles. Surge phase image pairs do not have unusually-high calculated uncertainties. We assume that these additional errors are stochastic and should not affect our conclusions.

TCD
6, 1181–1204, 2012

3.3 Surge dynamics

3.3.1 Velocity results

Between November 2007 and early March 2008, BGS velocities were consistently $\sim 1\,\mathrm{m\,d^{-1}}$ (Fig. 2) (30–110 km). In late March–April 2008, flow velocities accelerated 20 %, to $1.2\,\mathrm{m\,d^{-1}}$ (at least between 100 and 130 km). This acceleration is confirmed by a concurrent increase in the number of icequakes observed by a seismic array placed on the BGS at 110 km (LeBlanc, 2009). Offset tracking results were unavailable for late spring and summer 2008, but the same seismic array (LeBlanc, 2009) found the number of icequakes increased by an order of magnitude in the first two weeks of May, indicating an onset of activity much greater than the previous year's spring speed up. Between September 2008 and February 2009 our results show progressive acceleration in the BIV and lower BGS. Maximum observed velocities were $\sim 7\,\mathrm{m\,d^{-1}}$ and observed in a side shear zone at 130 km in February 2009. Centerline velocities were unavailable at 130 km. In January–April 2010 surface velocities from 110–140 km slowed to quiescent speeds but higher velocities remained in the lower BIV and close to the terminus. BIV velocities gradually accelerated between January and May 2010 (Figs. 1 and 2).

Unfortunately no SAR data was obtainable for the rest of 2010; but visual observations found decreasing crevassing until winter 2011 when classic surge morphology (Herzfeld and Mayer, 1997) appeared again on the BGS (Larsen, 2011; Molnia and Angeli, 2011). These observations suggest close to quiescent velocities throughout the summer and fall 2010 and a second high-velocity phase beginning in winter 2011 (Larsen, 2011; Molnia and Angeli, 2011). Surge morphology continued through summer 2011, and smoothed out in fall 2011, indicating quiescent flow.

A TerraSAR-X pair, obtained on 5–16 July 2011, captured an 11-day interval of velocities on Bering during the second phase (Fig. 3). The high resolution of TerrSAR-X reveals multiple arcuate propagation fronts on the glacier surface (Fig. 3) with velocities exceeding $9\,\mathrm{m\,d^{-1}}$. Observed longitudinal strain rates across the fronts exceed

TCD
6, 1181–1204, 2012

$6\,a^{-1}$ but are likely much higher in reality due to smoothing effects of the offset tracking routine.

These propagation fronts appear as extreme variability in the longitudinal profiles (Fig. 2). While these smaller fronts are quite evident, the velocity data do not show evidence of a uniform propagation front moving across the length of the BGS. Such a front would show a temporal delay in acceleration as one moves upstream. If we examine the period of acceleration between January 2008 and February 2009 at two locations (the lower BIV (80–90 km) and the BGS piedmont (110–130 km)) we see that the BIV reaches 45 % and 86 % of its peak velocity at the same time that the BGS piedmont reaches 33 % and 70 % if its peak velocity, respectively (Fig. 2). Therefore, the BIV reached a higher percentage of its total acceleration earlier than the BGS piedmont. Given the variability within the velocity data, we interpret this to mean that the BIV accelerated at least in unison with the lower Bagley, if not before.

We cannot make the same comparison with the WB due to lack of data. However, the WB accelerated in unison with the BGS in February 2008 – measurable acceleration (up to 26 %) extended 20 km upstream of the confluence (Figs. 2 and 4). The WB was back to quiescent velocities in November 2008, at the same time the BGS was accelerating rapidly. It accelerated again January 2009 when the BGS was flowing $7\,m\,d^{-1}$. By 2010, BGS velocities had slowed but the WB continued to accelerate.

3.3.2 Changes in surface elevation

During a surge, accelerated velocities move mass downstream from the upper reaches of a glacier, consequently thinning the glacier at the top of the surge (draw-down) and thickening the glacier at the bottom. The point separating thinning and thickening is called the dynamic balance line (Raymond, 1987). Surface mass balance also contributes to surface thinning/thickening. Negative mass balance typically causes gradually more thinning as one moves downstream. Altimetry data extends back to the end of the previous surge in 1995, with intervals of 5, 3 and 4 yr during the quiescent phase

TCD
6, 1181–1204, 2012

and one year intervals during the surge. Figure 5a presents both the rate of surface elevation change over each observation interval, and the total cumulative elevation change from 1995 to 2007 (only the quiescent phase).

3.3.3 Quiescent phase

As discussed earlier, during the quiescent phase of a surging glacier we expect the glacier geometry to re-steepen and increase driving stresses. Figure 5a presents observed changes in surface height and glacier geometry. Figure 5b presents the resultant changes in driving stresses during quiescent phase. We derive driving stress (Eq. 1) assuming a slope angle and thickness. For a rough approximation, thicknesses were assumed to be the surface elevation from the terminus to the equilibrium line (bed surface is close to sea level, Conway et al., 2009). Above the equilibrium line, we assume a linear decrease in thickness to zero at the divide. Slope angles were derived from the ASTER GDEM, using 6 km boxcar smoothing to remove small-scale variation and data artifacts. We assume that this DEM represents the glacier surface in 1995, and sequentially adjust the geometry with the altimetry data. Our crude assumptions on ice thickness will not affect our conclusions, because temporal changes in driving stress are sensitive primarily to the changing geometry provided by the altimetry.

Between 1995 and 2003, the accumulation area thickened slightly, the ablation area thinned and driving stresses increased slightly in the BIV and upper Bering. Over the 1995–2000 interval, a small acceleration event occurred (1995–2000 interval) that redistributed some of the newly accumulated mass downstream and consequently steepened the geometry and increased driving stresses between 120 and 130 km (grey highlight in Fig. 5). Between 2003 and 2007, a larger acceleration event occurred, this time further up-glacier, which drew down in the accumulation zone and thickened Bering Glacier by about 20 m between 85 and 120 km. This event also steepened the surface slope in the same location, between 120 and 130 km (grey highlight in Fig. 5). Over the entire quiescent phase, all new/added mass in the accumulation zone was redistributed to a small region between 85 and 120 km. Consequently, when the surge began in

TCD
6, 1181–1204, 2012

2008, driving stresses immediately downstream of the thickening had increased ~ 70 % (or ~ 50 kPa) since 1995 (grey highlight in Fig. 5b). But elsewhere on the BGS, driving stresses in 2008 were nearly identical to 1995.

The area where driving stresses increased during quiescent phase was also key during the surge. It was the location of dynamic balance line during the first phase of the surge. It had the strongest acceleration and fastest velocities in the first phase (Figs. 2 and 5a). Finally, it was the approximate location that the 1993–1995 surge is thought to have initiated (Roush, 2003).

3.3.4 Surge phase

Surge onset is captured in the 2007–2008 interval, while the main portion of the first phase occurred during the 2008–2009 interval (Fig. 5a). Throughout the first stage, drawdown extended from ~ 80 to 120 km, has similar magnitude (though opposite sign) and distribution of the thickening that occurred during quiescent phase.

Thinning (thickening) upstream (downstream) of 123 km suggests that maximum ice displacements occurred around 123 km throughout the first phase (assuming a simple 1-dimensional case, barring surface mass balance; Patterson, 2010). While velocities were peaking in 2008–2009, the surge pushed ~ 15 km downstream nearly reaching the terminus (Fig. 5a). In 2008–2009, a local maximum in thickening at 130 km is spatially coincident with the maximum thickening in 2007–2008 and the steepening point during the quiescent phase.

The 2009–2010 interval includes what we define as the end of the first phase. The surge slowed and the longitudinal velocity profile became bi-modal (Fig. 2). Surface height increases are close to the terminus (Fig. 5), which is consistent with elevated velocities at 150 km in 2010 (Fig. 2). The accelerated velocities in the BIV in 2010 caused drawdown in the BIV but no surface elevation increases are seen directly downstream. This suggests that accelerated speeds from 100–140 km continued into fall of 2009 before settling to quiescent speeds in January 2010.

TCD
6, 1181–1204, 2012

3.3.5 Surge dynamics in the BIV

During 2008–2010 and 1993–1995, the BGS accelerated longitudinally from a point 45 km below the ice-divide (Fig. 2). Upstream of 45 km, surge velocities remained close to quiescent velocities. Downstream of 45 km, rapid longitudinal acceleration occurred in a step-like fashion. Strain rates (not shown) indicate the peak at 80 km (Fig. 2) is caused by longitudinal compression as the BIV joins with the WB. The cause of the deceleration at 65 km is less clear but is probably due to bed topography. At this point, there is extensional lateral strain as ice spreads northward and compresses ice on the north side of the BIV.

The north side of the BIV receives its ice from the Jefferies Glacier, which eventually flows into the Tana (Fig. 1). This ice accelerated very little – from 0.5 to 0.7 $\mathrm{m\,d^{-1}}$ – during the BGS surge. A wider shear zone on the north side of the BIV is visible in Fig. 1. Also notable, the longitudinal step-like accelerations seen on the Bering portion of the BIV, did not occur on ice originating from the Jefferies Glacier (Figs. 1 and 2). Rather, velocities were relatively uniform from the Jefferies to the Tana. The Bagley fault runs along the BIV and possibly forms a longitudinal ridge structure that separates BGS ice and the Tana Glacier ice. This structure likely extends towards the north edge of the West Bagley and diverts the majority of the ice southward into Bering (Plafker, 1987; Bruhn et al., 2004). Flow velocities on the Tana Glacier changed by only $\sim 0.1\,\mathrm{m\,d^{-1}}$ throughout the 2008–2010 BGS surge; the highest velocities were actually prior to the surge, in 2007.

4 Conclusions

The Bering began a full-scale surge in May 2008 that appears to have ended in summer 2011. The quiescent phase has some similarities to that observed on the Medvezhiy Glacier in Tajikistan by Dolgushin and Osipova (1978) (see also Raymond, 1987). During quiescent phase, thickening in the accumulation area caused slight increases in

TCD
6, 1181–1204, 2012

driving stress. The increase in driving stress causes slight acceleration in the accumulation zone and consequent thickening where the accelerated front approaches stagnant ice downstream. Dolgushin and Osipova (1978) saw this same process – a steepening and advancing front during quiescent phase – on the Medvezhiy Glacier (Raymond, 1987). The fact the front on Bering didn't develop much during the 2000–2003 interval suggests that the acceleration isn't purely a consequence of increased driving stresses and that bed conditions likely play a role as well.

Given the localized increases in driving stresses during the quiescent phase, it would seem logical for a surge to initiate at ~ 125 km and propagate upstream and downstream. While we do see the highest velocities at 125 km, it is interesting that, initially, the BGS accelerated as a whole between ~ 50–140 km. Accelerated velocities did propagate upstream and downstream as is evident in the altimetry data, but these data are over year-long intervals. The surge didn't reach the terminus until sometime in 2009 and didn't propagate into the BIV until even later, in 2010. Thus, we suggest that the synchronous acceleration observed in 2008 is the result of hydrologic pressurization of the bed in May 2008 that extended from at least 140 km up into the BIV. The pressurization led to decreased basal stresses and synchronous acceleration, of at least modest magnitudes (not a true surge, yet), throughout the glacier length. Rapid acceleration and the "surge" initiated in the one area (120–130 km) with sufficiently high driving stresses and bed conditions that facilitate non-linear acceleration. The surge then propagated upstream and downstream as the high velocities redistributed driving stress by steepening the geometry along propagation fronts.

Though we don't have robust data to evaluate propagation velocities, we can note the locations of drawdown and thickening within each interval in the altimetry data. It is interesting that while the thickening moved downstream significantly in 2009, the majority of the drawdown did not move upstream at all. We suggest this occurred because of the thickening bulge that occurred during quiescent phase, between 80 and 120 km. Since the surge initiated downstream of this bulge, drawdown would have to move much of this mass before driving stresses could be significantly increased in

TCD
6, 1181–1204, 2012

the BIV. As can be observed in Fig. 5a, this occurred sometime in late 2009 and the propagation front was able to move further upstream in 2010.

It is interesting that the first acceleration period lasted at least ten months (May 2008–February 2009) and took place primarily in fall, when glacier flow rates are typically at a seasonal low. Also note that this progressive acceleration occurred after an exceptionally cold summer (Alaska Climate Research Center, 2012). However, the cold summer was not responsible for triggering the surge, as the onset occurred in May.

We find that the active surge zone of the BGS extends throughout Bering Glacier but is confined to an area downstream of the Jefferies Glacier confluence in the BIV. Upstream of the confluence, ice may accelerate slightly due to longitudinal extension and drawdown, but surge velocities (1993–1995 and 2008–2010) and quiescent velocities (2007) vary by little ($< 0.35\,\mathrm{m\,d^{-1}}$). We suggest that the bed type changes at this point, perhaps from a solid bed upstream of the active surge zone to a deformable bed in the active surge zone. A strike-slip fault boundary runs though the BIV and WB (Plafker, 1987; Bruhn et al., 2004) and would provide easily erodible conditions for generation of till (Harrison and Post, 2003). It is also notable that the active surge zone appears to be confined to ice in the Southern BIV, which flows into the Bering and does not include ice flowing into the Tana Glacier.

Finally, ice dynamics on the north side of the BIV and the Tana Glacier appear to operate independently of the BGS and do not accelerate when the south BIV, WB or Bering does. This could be due to a lack of a deformable bed and/or an independent sub-glacial hydrologic system.

Acknowledgements. We thank Ron Bruhn, Jeanne Sauber, James Turrin, and Michelle Cotton for their insightful ideas and discussion. E. Burgess is funded under the NASA Earth Science Space Fellowship. R. Forster and the velocity work was funded by NASA Grants NNX08AP27G and NNX08AX88G. C. Larsen and UAF LiDAR altimetry program were funded by NASA's Operation Ice Bridge Grant NNH09ZDA001N (2010), NASA Grant NNX09AP54G (2009), NSF ARC-0612537 (2008), and NASA Grant NNH07ZDA001N-CRYO (2007). M. Braun was supported by NASA Grant NNX11AF41G and TerraSAR-X data was provided under DLR AO LAN_0164.

TCD
6, 1181–1204, 2012

References

Alaska Climate Research Center: available at: http://climate.gi.alaska.edu/Climate/Location/TimeSeries/Yakutat.html, last access: 10 February, 2012.

Arendt, A. A., Echelmeyer, K. A., Harrison, W. D., Lingle, C. S., and Valentine, V. B.: Rapid wastage of Alaska glaciers and their contribution to rising sea level, Science, 297, 382–386, doi:10.1126/science.1072497, 2002.

Arendt, A., Echelmeyer, K., Harrison, W., Lingle, C., Zirnheld, S., Valentine, V., Ritchie, B., and Druckenmiller, M.: Updated estimates of glacier volume changes in the Western Chugach Mountains, Alaska, and a comparison of regional extrapolation methods, J. Geophys. Res., 111, F03019, doi:10.1029/2005JF000436, 2006.

Arendt, A. A., Luthcke, S. B., Larsen, C. F., Abdalati, W., Krabill, W. B., and Beedle, M. J.: Validation of high-resolution GRACE mascon estimates of glacier mass changes in the St. Elias Mountains, Alaska, USA, using aircraft laser altimetry, J. Glaciol., 54, 778–787, doi:10.3189/002214308787780067, 2008.

Armstrong, R., Raup, B., Khalsa, S. J. S., Barry, R. G., Kargel, C., and Kieffer, H.: GLIMS Glacier Database, National Snow and Ice Data Center, Boulder, Colorado, 2005.

Beedle, M. J., Dyurgerov, M., Tangborn, W., Khalsa, S. J. S., Helm, C., Raup, B., Armstrong, R., and Barry, R. G.: Improving estimation of glacier volume change: a GLIMS case study of Bering Glacier System, Alaska, The Cryosphere, 2, 33–51, doi:10.5194/tc-2-33-2008, 2008.

Berthier, E., Schiefer, E., Clarke, G. K. C., Menounos, B., and Rémy, F.: Contribution of Alaskan glaciers to sea-level rise derived from satellite imagery, Nat. Geosci., 3, 92–95, 2010.

Bindschadler, R., Vornberger, P., Blankenship, D., Scambos, T., and Jacobel, R.: Surface velocity and mass balance of ice streams D and E, West Antarctica, J. Glaciol., 42, 461–475, 1996.

Bruhn, R. L., Pavlis, T. L., Plafker, G., and Serpa, L.: Deformation during terrane accretion in the Saint Elias orogen, Alaska, B. Geol. Soc. Am., 116, 771–787, doi:10.1130/B25182.1, 2004.

Dolgushin, L. D. and Osipova, G. B.: Balance of a surging glacier as the basis for forecasting its periodic advances, Mater. Glyatsiologicheskikh Issled, Khronica Obsuzhdeniya, 32, 260–265, 1978.

Echelmeyer, K. A., Harrison, W. D., Larsen, C. F., Sapiano, J., Mitchell, J. E., Demallie, J., Rabus, B., Adalgeirsdóttir, G., and Sombardier, L.: Airborne surface profiling of glaciers: a case-study in Alaska, J. Glaciol., 42, 538–547, 1996.

TCD
6, 1181–1204, 2012

Fatland, D. R. and Lingle, C. S.: Analysis of the 1993–1995 Bering Glacier (Alaska) surge using differential SAR interferometry, J. Glaciol., 44, 532–546, 1998.
Fatland, D. R. and Lingle, C. S.: InSAR observations of the 1993–1995 Bering Glacier (Alaska, USA) surge and a surge hypothesis, J. Glaciol., 48, 439–451, doi:10.3189/172756502781831296, 2002.
Gray, A. L., Mattar, K. E., Vachon, P. W., Bindschadler, R., Jezek, K. C., Forster, R., and Crawford, J. P.: InSAR results from the RADARSAT Antarctic mapping mission data: estimation of glacier motion using a simple registration procedure, Int. Geosci. Remote Sens. Symp., 3, 1638–1640, 1998.
Harrison, W. D. and Post, A. S.: How much do we really know about glacier surging?, Ann. Glaciol., 36, 1–6, 2003.
Herzfeld, U. C. and Mayer, H.: Surge of Bering Glacier and Bagley Ice Field, Alaska: an up date to August 1995 and an interpretation of brittle deformation patterns, J. Glaciol., 43, 427–434, 1997.
Kamb, B., Raymond, C. F., Harrison, W. D., Engelhardt, H., Echelmeyer, K. A., Humphrey, N., Brugman, M. M., and Pfeffer, T.: Glacier surge mechanism: 1982–1983 surge of variegated glacier, Alaska, Science, 227, 469–479, doi:10.1126/science.227.4686.469, 1985.
Koenig, L., Martin, S., Studinger, M., and Sonntag, J.: Polar airborne observations fill gap in satellite data, Eos Trans. AGU, 91, 333, doi:10.1029/2010EO380002, 2010.
Larsen, C. F.: Chris Larsen Photography – Bering Glacier – 4 April 2011, available online at: http://www.gps.alaska.edu/chris/images/Bering_2011.4.11/index.html, last access: 17 January 2012, 2011.
LeBlanc, L.: Icequakes and ice motion: a time-series analysis of the dynamics of the bering glacier, Alaska, M.Sc. thesis, Geophysical Institute, University of Alaska Fairbanks, Fairbanks, Alaska, 2009.
Maronna, R. A.: Robust Statistics: Theory and Methods, J. Wiley, Chichester, England, 2006.
Meier, M. F. and Post, A. S.: What are glacier surges?, Can. J. Earth Sci., 6, 807–817, 1969.
Michel, R. and Rignot, E.: Flow of Glaciar Moreno, Argentina, from repeat-pass shuttle imaging radar images: comparison of the phase correlation method with radar interferometry, J. Glaciol., 45, 93–100, 1999.
Molnia, B.: Glaciers of North America – Glaciers of Alaska, in: Satellite Image Atlas of Glaciers of the World, US Geological Survey Professional Paper 1386-K, edited by: Williams, R. S. and Ferrigno, J. G., United States Government Printing Office, Washington, 525 pp., 2008.

TCD
6, 1181–1204, 2012

Molnia, B. and Angeli, K.: Comparison of the 2008–2011 and 1993–1995 surges of Bering Glacier, Alaska, AGU Fall Meeting, San Francisco, CA, 2011.
Muskett, R. R., Lingle, C. S., Tangborn, W. V., and Rabus, B. T.: Multi-decadal elevation changes on Bagley Ice Valley and Malaspina Glacier, Alaska, Geophys. Res. Lett., 30, 1857, doi:10.1029/2003GL017707, 2003.
Nye, J. F.: A method of determining the strain-rate tensor at the surface of a glacier, J. Glaciol., 3, 409–419, 1959.
Paterson, W. S. B.: Physics of Glaciers, 4th edn., Butterworth-Heinemann, Burlington, MA, 2010.
Plafker, G.: Regional geology and petroleum potential of the northern Gulf of Alaska continental margin, in: Geology and Resource Potential of the Continental Margin of Western North America and Adjacent Ocean Basins, edited by: Scholl, D. W., Grantz, A., and Vedder, J. G., Circum-Pacific Council for Energy and Mineral Resources, Houston, TX, 229–268, 1987.
Post, A.: Periodic surge origin of folded medial moraines on Bering Piedmont Glacier, Alaska, J. Glaciol., 11, 219–226, 1972.
Raymond, C. F.: How do glaciers surge? A review, J. Geophys. Res., 92, 9121–9134, 1987.
Raymond, C. F. and Harrison, W. D.: Evolution of variegated glacier, Alaska, USA prior to its surge, J. Glacio., 34, 154–169, 1988.
Roush, J. J., Lingle, C. S., Guritz, R. M., Fatland, D. R., and Voronina, V. A.: Surge-front propagation and velocities during the early-1993–95 surge of Bering Glacier, Alaska, USA, from sequential SAR imagery, Ann. Glaciol., 36, 37–44, doi:10.3189/172756403781816266, 2003.
Strozzi, T., Luckman, A., Murray, T., Wegmuller, U. and Werner, C. L.: Glacier motion estimation using SAR offset-tracking procedures, IEEE T. Geosci. Remote Sens., 40, 2384–2391, doi:10.1109/TGRS.2002.805079, 2002.

TCD
6, 1181–1204, 2012

Table 1. Statistics describing the 2-D distribution of measured ground displacements in ice-free terrain (units in md^{-1}). The STDEV, MADn, IQR, and absolute median are calculated for all stable-ground offsets within each image pair. Table 1 shows the mean statistics (STDEV, MADn, IQR and absolute median) for all image pairs.

	RADARSAT		PALSAR	
	Range	Azimuth	Range	Azimuth
Mean STDEV	0.251	0.259	0.094	0.081
Mean MADn	0.033	0.033	0.024	0.013
Mean IQR	0.045	0.045	0.033	0.017
Mean Absolute MEDIAN	0.005	0.009	0.006	0.002

TCD
6, 1181–1204, 2012

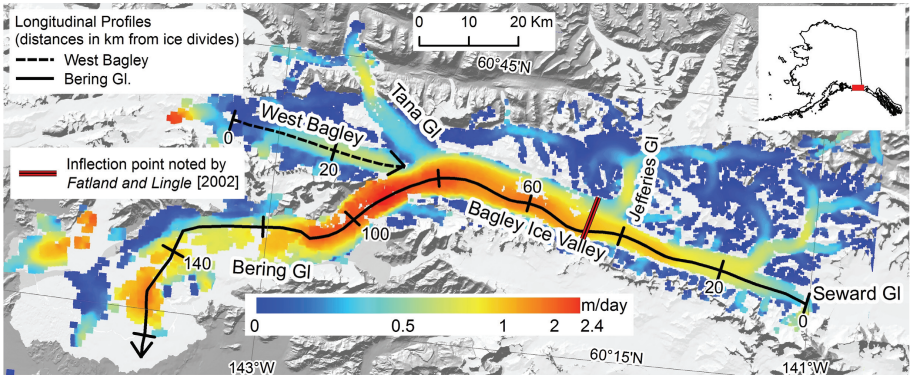

Fig. 1. Composite velocity map of the BGS, WB, Tana Glacier and Jefferies Glacier in Winter 2010. BGS and WB longitudinal profiles apply to Figs. 2 and 3, respectively. White glacier outline provided by Armstrong et al. (2005).

TCD
6, 1181–1204, 2012

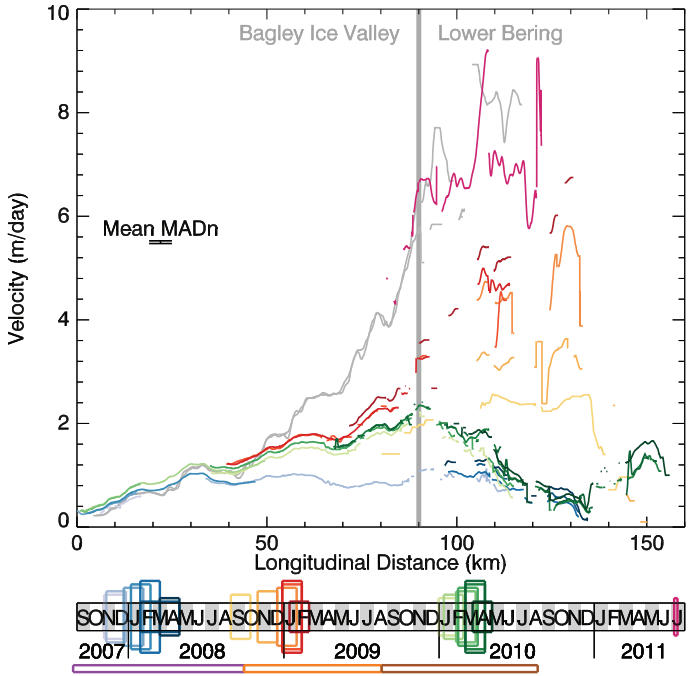

Fig. 2. Bering Glacier System longitudinal velocity profile (location in Fig. 1). Dates of image pairs are denoted in timeline. Colors gradually darken as time moves forward each winter. Bars below the timeline show dates of altimetry intervals in Fig. 4. BGS velocities in January 1994 (grey data line). Division between the BIV and Bering denoted by vertical grey bar.

TCD
6, 1181–1204, 2012

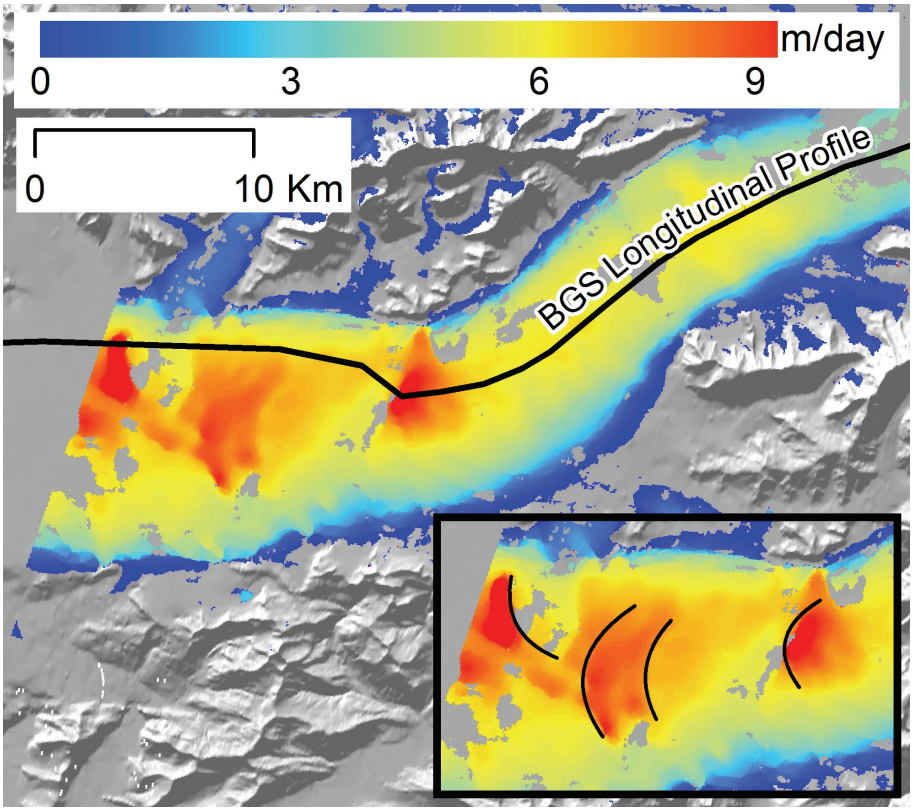

Fig. 3. High-resolution velocity field during second phase of the surge over 11 day interval (5–16 July 2011) from TerraSAR-X. Location of propagation fronts marked in inset map.

TCD
6, 1181–1204, 2012

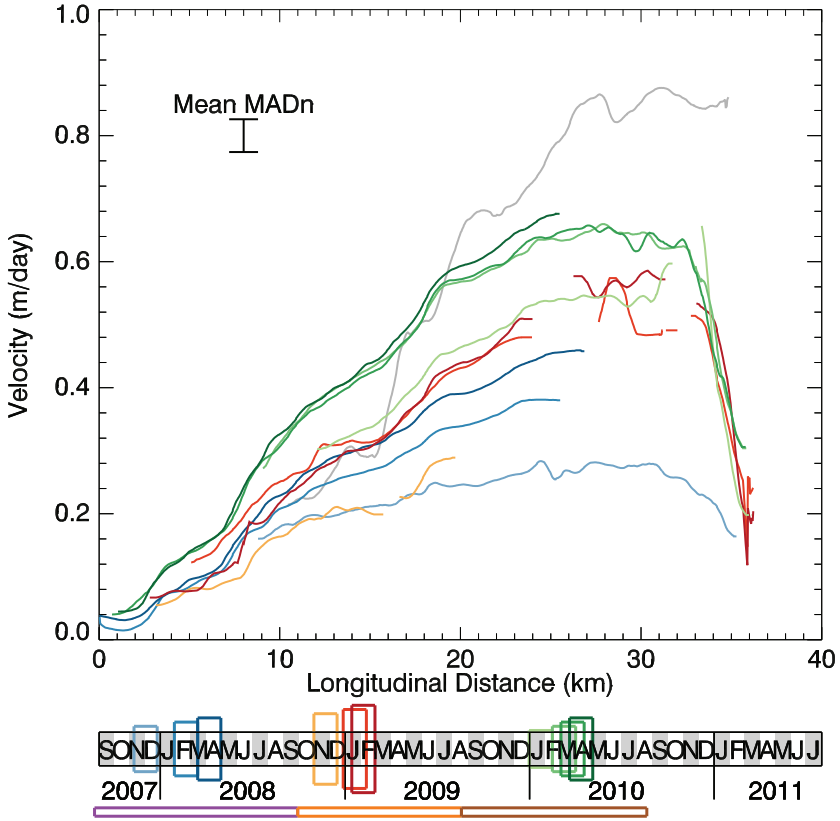

Fig. 4. West Bagley longitudinal velocity profile (location in Fig. 1). Dates of each image pair are denoted in the timeline below. Colors gradually darken as time moves forward each winter. The grey data line shows WB velocities in January 1994. Note scales are different than Fig. 2.

TCD
6, 1181–1204, 2012

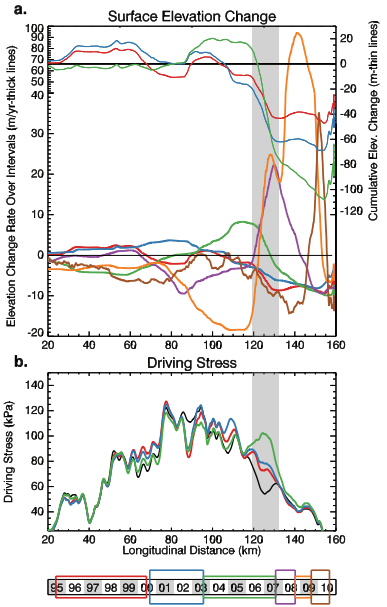

Fig. 5. Airborne LiDAR altimetry data and calculated driving stresses along the BGS longitudinal profile (Fig. 1). Dates of altimetry flight intervals show at bottom. **(a)** Surface elevation change along BGS longitudinal profile. Thick lines denote elevation change rate over each flight interval. Thin lines denote total cumulative elevation change after each interval from 1995 and are only shown during quiescent phase to address steepening glacier geometry. X-axis is approximately equivalent to that in Figs. 2 and 4, flight path was within < 2 km of the Bering centerline. Note compressed y-axis above 40 m yr^{-1}. **(b)** Driving stress derived from thickness and glacier slope angle for quiescent phase only (Eq. 1). Black line applies to geometry in 1995, colored lines indicate driving stress after each respective flight interval.

TCD
6, 1181–1204, 2012